

Numerical Simulations of Heat and Moisture Transport in Thermal Protective Clothing Under Flash Fire Conditions

Guowen Song

Department of Human Ecology, University of Alberta, Edmonton, Canada

Patirop Chitrphiromsri

College of Textiles, North Carolina State University, Raleigh, USA

Dan Ding

Department of Human Ecology, University of Alberta, Edmonton, Canada

A numerical model of heat and moisture transport in thermal protective clothing during exposure to a flash fire was introduced. The model was developed with the assumption that textiles are treated as porous media. The numerical model predictions were compared with experimental data from different fabric systems and configurations. Additionally, with the introduction of a skin model, the parameters that affect the performance of thermal protective clothing were investigated.

numerical model protective clothing moisture transport flash fire condition skin model

1. INTRODUCTION

Heat and moisture transfer in porous media are common phenomena with wide applications in engineering fields, such as civil engineering, energy conservation, textiles, and functional garment design [1]. Field study and research performed during the past 10 years have demonstrated that the presence of moisture in textiles significantly affects the performance of textiles and garments [2, 3, 4, 5, 6]. In developing thermal protective clothing materials, such as firefighter garments, researchers have traditionally focused on heat transfer in dry

conditions. However, moisture transport in fabrics and its effect on the protective performance of the garment have not been studied in sufficient detail. Textile fabric can be treated as a porous medium. Heat and mass transport in wet porous media are coupled in a complicated way. Energy transport in such a medium occurs by radiation and conduction in all phases as well as by convection within the liquid and gas phases. There are many models for analyzing multiphase transport in porous media. Vafai and Sözen summarized and compared these models [7]. Gibson's model described fabrics subjected to intensive heat [8]. Gibson

Data in this article were generated to characterize the properties of materials or assemblies in response to thermal exposure under controlled laboratory conditions or in model predictions. They should not be used to appraise materials, products or assemblies under actual fire conditions. They are not presented to predict all types of field conditions where the nature of thermal exposure can be physically complicated and unqualified. We wish to emphasize that it is not our intention to recommend, exclude or predict the suitability of any commercial product for a particular end-user.

Correspondence and requests for offprints should be sent to Guowen Song, Protective Clothing & Equipment Research Facility, Department of Human Ecology, 331 Human Ecology Building, University of Alberta, Edmonton, AB T6G 2N1, Canada. E-mail: <guowen.song@ualberta.ca>.

analyzed multiphase transport in hygroscopic porous textiles. However, Gibson’s model did not consider radiation heat transfer within the fabric layer. Torvi developed a one-dimensional transient heat transfer model, which accounts for the penetrating radiative heat transfer through a fabric [9]. In this research, a model that couples heat and moisture transport for multilayer protective fabrics under flash fire conditions is introduced and the effect of heat and moisture transport on the performance of thermal protective clothing is analyzed.

2. MATHEMATICAL MODEL FORMULATION

Figure 1 illustrates a multilayer protective fabric system exposed to a high-intensity flash fire. This

garment system consists of three different fabric layers, i.e., an outer shell, a moisture barrier, and a thermal liner, respectively, from the exterior to the interior of the clothing ensemble. An air gap between the inner layer of the fabric and the heat flux sensor is introduced.

2.1. Heat and Moisture Transport in Textile Material

Textile fabrics can be modeled as hygroscopic porous media. The porous textile material is a mixture of a solid phase consisting of solid fibers and bound water absorbed by a solid polymer matrix, and a gaseous phase consisting of water vapor and dry air. A schematic diagram of the structure of a porous textile is demonstrated in Figure 2. Gibson [8] developed a set of equations for modeling heat and mass

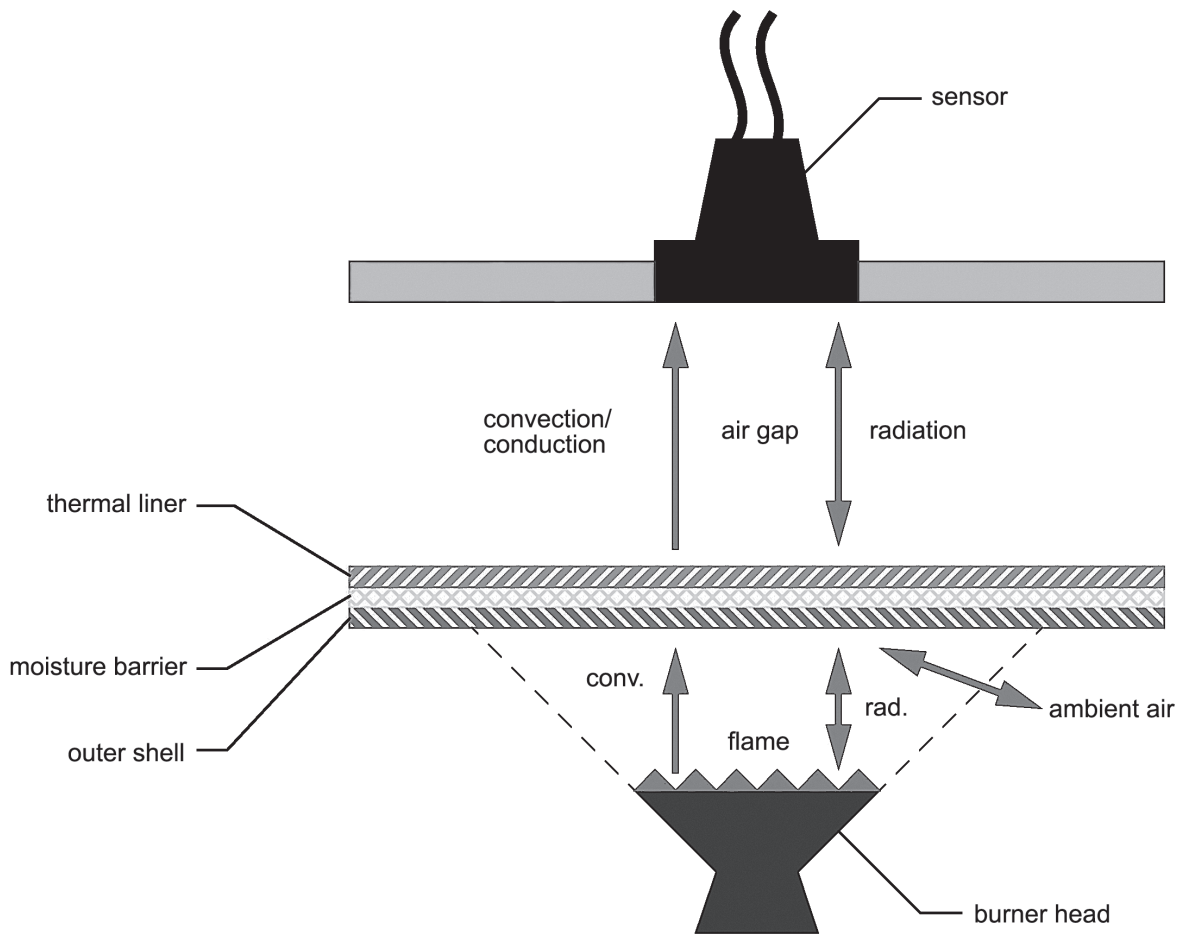


Figure 1. Schematic diagram of protective clothing fabric and the thermal protective performance (TPP) sensor. Notes. conv.—convection, rad.—radiation.

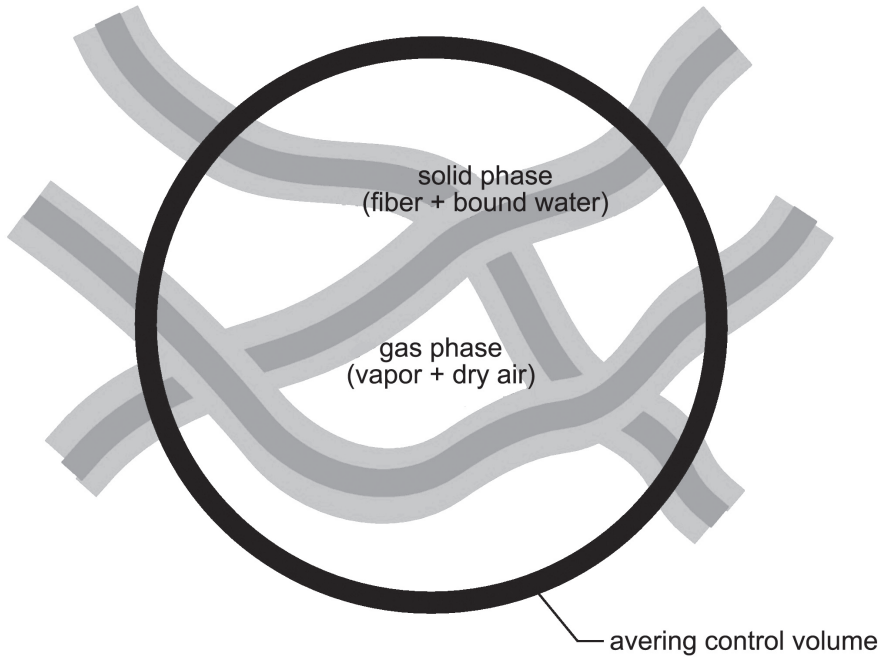


Figure 2. Schematic diagram of a two-phase structure of porous textile media in the averaging control volume.

transfer through textile materials by applying Whitaker’s [10] theory of coupled heat and mass transfer through porous media. Torvi’s model assumed that convective heat flux only applied to the surface of the fabric but radiative heat flux could penetrate through the fabric up to a certain depth [9]. Morton and Hearle gave definitions of the physical properties of the fabric [11]. The convective heat transfer in the air gap between the fabric and the sensor was simulated as natural convection in a horizontal enclosure, which was heated from below [12]. Based on those assumptions, the energy balance in the infinitesimal element of the fabric can be formulated in the form of a differential equation. A partial differential equation is developed for temperature distribution in a composite fabric layer by combining Gibson’s and Torvi’s models. Therefore, the energy equation is modeled on Gibson’s model and penetrating radiation, a term described by Torvi’s model. Thermal properties of all phases are accounted for in the model based on the relations given by Gibson. Radiative heat transfer in the fabric is accounted for by introducing in the energy equation a source term similar to that in Torvi’s model. Gas phase

convection contributions caused by pressure differences, which can arise either due to body movement or due to external air movement, are neglected. Moreover, it is assumed that if there is any extra liquid sweat which builds up on the surface of the sensor (skin), it will either drip off or wick into the fabric and then it will be absorbed by the fabric fibers and become bound water. In other words, free liquid water exists neither on the surface of the sensor nor in the fabric layer.

The energy equation can be formulated as

$$\begin{aligned} &\rho c_p \frac{\partial T}{\partial t} + (\Delta h_l + \Delta h_{\text{vap}}) \dot{m}_{\text{sv}} \\ &= \frac{\partial}{\partial x} \left(k_{\text{eff}} \frac{\partial T}{\partial x} \right) + \gamma \cdot q_{\text{rad}}'' e^{-\gamma x}, \end{aligned} \tag{1}$$

where ρ —effective density of the fabric, c_p —effective specific heat of the fabric, T —temperature, t —time, Δh_l —enthalpy of transition per unit mass from bound water to free liquid water, Δh_{vap} —enthalpy of evaporation per unit mass, \dot{m}_{sv} —mass flux of vapor out of the fiber (or into the fiber if \dot{m}_{sv} is negative), x —linear vertical co-ordinate, k_{eff} —effective thermal conductivity of the fabric, γ —extinction coefficient of the fabric, and q_{rad}'' —incident

radiation heat flux from the flame onto the fabric. Chitrphiromsri and Kuznetsov provide details on the development of the model and its relevant parameters [13].

The solid phase continuity equation can be described as

$$\rho_w \frac{\partial}{\partial t} (\varepsilon_{bw}) + \dot{m}_{sv} = 0. \quad (2)$$

The gas phase diffusivity equation can be written as

$$\frac{\partial}{\partial t} (\varepsilon_\gamma \rho_v) - \dot{m}_{sv} = \frac{\partial}{\partial x} \left(D_{\text{eff}} \frac{\partial \rho_v}{\partial x} \right), \quad (3)$$

where D_{eff} —effective diffusivity of the gas phase in the fabric, which is defined [8] from

$$D_{\text{eff}} = \frac{D_a \varepsilon_\gamma}{\tau}, \quad (4)$$

where D_a —diffusivity of water vapor in the air and τ —fabric tortuosity.

Boundary conditions for the fabric:

$$-k_{\text{eff}} \frac{\partial T}{\partial x} \Big|_{x=0} = (q''_{\text{conv}} + q''_{\text{rad}})_{x=0}; \quad (5)$$

$$-k_{\text{eff}} \frac{\partial T}{\partial x} \Big|_{x=L_{\text{fab}}} = (q''_{\text{air,rad}} + q''_{\text{air,cond/conv}})_{x=L_{\text{fab}}}, \quad (6a)$$

with-air-gap configuration;

$$-k_{\text{eff}} \frac{\partial T}{\partial x} \Big|_{x=L_{\text{fab}}} = h_i (T_{\text{fab}} \Big|_{x=L_{\text{fab}}} - T_{\text{sens}}), \quad (6b)$$

without-air-gap configuration;

$$h_{m,\text{amb}} (\rho_{v,\text{amb}} - \rho_v)_{x=0} = -D_{\text{eff}} \frac{\partial \rho_v}{\partial x} \Big|_{x=0}; \quad (7a)$$

$$h_{m,\text{gap}} (\rho_v - \rho_{v,\text{air}})_{x=L_{\text{fab}}} = -D_{\text{eff}} \frac{\partial \rho_v}{\partial x} \Big|_{x=L_{\text{fab}}}, \quad (7b)$$

with-air-gap configuration;

$$-D_{\text{eff}} \frac{\partial \rho_v}{\partial x} \Big|_{x=L_{\text{fab}}} = 0, \text{ without-air-gap configuration}; \quad (7c)$$

where q''_{conv} —convective heat flux from the flame to the fabric, $q''_{\text{air,rad}}$ —heat flux by radiation from the fabric to the sensor across the air gap, $q''_{\text{air,cond/conv}}$ —heat flux by conduction/convection from the fabric to the sensor across the air gap, h_i —interfacial conductance between the inner surface of the fabric and the sensor, $T_{\text{fab}} \Big|_{x=L_{\text{fab}}}$ —temperature on the inside surface of the fabric, T_{sens} —temperature on the surface of the sensor, h_m —convective mass transfer coefficient,

$\rho_{v,\text{amb}}$ —density of water vapor in the ambient air, and $\rho_{v,\text{air}}$ —density of water vapor in the air gap.

According to Torvi [9] the radiation and convection heat fluxes from the flame to the fabric are

$$(q''_{\text{conv}} + q''_{\text{rad}})_{x=0} = h_{c,\text{fl}} (T_g - T_{\text{fab}} \Big|_{x=0}), \quad (8)$$

where $h_{c,\text{fl}}$ —convective heat transfer coefficient between the flame and the outer surface of the fabric. The heat flux by radiation from the fabric to the sensor across the air gap is

$$q''_{\text{air,rad}} \Big|_{x=L_{\text{fab}}} = \frac{\sigma (T_{\text{fab}} \Big|_{x=L_{\text{fab}}}^4 - T_{\text{sens}}^4)}{\left(\frac{1}{\tilde{\varepsilon}_{\text{fab}}} + \frac{1 - \tilde{\varepsilon}_{\text{sens}}}{\tilde{\varepsilon}_{\text{sens}}} \right)}, \quad (9)$$

where $\tilde{\varepsilon}_{\text{sens}}$ —emissivity of the sensor. Torvi also gives the heat flux by conduction/convection from the fabric to the sensor across the air gap:

$$q''_{\text{air,cond/conv}} \Big|_{x=L_{\text{fab}}} = h_{c,\text{gap}} (T_{\text{fab}} \Big|_{x=L_{\text{fab}}} - T_{\text{sens}}), \quad (10)$$

where $h_{c,\text{gap}}$ —convective heat transfer coefficient of the air due to conduction and natural convection in the air gap, which is

$$h_{c,\text{gap}} = Nu \frac{k_{\text{air}}(T)}{L_{\text{gap}}}, \quad (11)$$

where Nu —Nusselt number; $k_{\text{air}}(T)$ —thermal conductivity of the air, which is a function of T only; and L_{gap} —thickness of the air gap [9].

2.2. Heat Transfer Into the Sensor

The heat flux, which applies to a sensor, is determined from a test temperature sensor on the basis of a lumped heat capacity analysis of the insulated copper sensor. The heat flux is modeled as

$$q''_{\text{sens}} = \left(\frac{m c_p}{\tilde{\varepsilon} A} \right)_{\text{sens}} \frac{dT}{dt}, \quad (12)$$

where m_{sens} —density of the sensor, $(c_p)_{\text{sens}}$ —specific heat of the sensor, and A_{sens} —surface area of the sensor.

Boundary conditions for the sensor:

$$q''_{\text{sens}} = (q''_{\text{air,rad}} + q''_{\text{air,cond/conv}})_{x=L_{\text{fab}}+L_{\text{gap}}}, \quad (13a)$$

with-air-gap configuration;

$$q''_{\text{sens}} = h_i (T_{\text{fab}} - T_{\text{sens}}), \text{ without-air-gap configuration.} \quad (13b)$$

2.3. Natural Convection in the Air Gap Between the Fabric and the Sensor

For modeling the thermal response of thermal protective clothing exposed to a flash fire in thermal protective performance (TPP) tests, convective heat transfer in the air gap between the fabric and the sensor is simulated as natural convection in a horizontal enclosure heated from below. Hollands, Unny, Raithby, and Konicek [12] presented the correlation for air in a horizontal enclosure heated from below:

$$Nu = 1 + 1.44 \left[1 - \frac{1708}{Ra} \right]^{\circ} + \left[\left(\frac{Ra}{5830} \right)^{\frac{1}{3}} - 1 \right]^{\circ} \quad (14)$$

The notation [][°] indicates that if the argument in the square brackets is negative, the quantity should be taken as zero.

2.4. Numerical Procedure

The finite volume method is adopted to solve the differential equations, which are the energy equation for the fabric, the solid phase continuity equation, the gas phase diffusivity equation, and the heat transfer equation for the sensor [14, 15]. The Crank-Nicholson scheme is applied to discretize the transient partial differential equations. Due to nonlinearities in this system, the Gauss-Seidel point-by-point iterative scheme is employed to solve these equations. To avoid divergence of the iteration method, the under-relaxation procedure is utilized. The value of the under-relaxation parameter is 0.8. The solution procedure is as follows: all variables are known at the initial state, then the program progresses in given time increments. The variables at the previous time step are used as guessed values for the variables at the current time step. The new values of variables are computed by visiting each grid point in a certain order. Then the iterations are repeated until the changes in the solutions become smaller than 10⁻⁶.

2.5. Determination of Fabric Thickness

Fabric thickness is evaluated by performing measurements with the Kawabata instrument. Thickness change depends on the applied load.

Nominal fabric thickness is chosen at the pressure of 10 gf/cm².

3. MODEL VALIDATION

To compare the prediction based on the model with experimental data, different fabric systems, from one- and two- to multilayer systems, were selected and tested in different configurations. The multilayer system consisted of three different fabric layers: an outer shell, a moisture barrier, and a thermal liner, from the exterior to the interior of clothing ensembles, respectively. The two-layer system included an outer shell and a moisture barrier, and the one-layer system consisted of a shell only. These fabric systems were exposed to a high-intensity flash fire simulation in a TPP [16] test configuration as shown in Figure 1. Kombat™ (60/40 Kevlar®/polybenzimidazole [PBI] blend) was the shell fabric of the garment system, ComfortZone™ (flame retardant polyurethane film on Basofil®/Aramid blend spunlace) was the moisture barrier, and Aralite® (Aramid batt quilted to Nomex®) was the thermal liner. The tests were performed under two test configurations: with and without an air gap. Nominal thickness of the air gap (0.00635 m; 1/4 in.) was adopted for the TPP test. Table 1 shows the thermophysical/geometrical properties of the fabric utilized in the computations. Table 2 lists the radiation parameters used in the computations [9]. Table 3 gives the thermophysical/geometrical properties of the TPP sensor. Table 4 details the thermal properties of the flame and the ambient air, and the initial data of the fabric and the air gap.

Figures 3 and 4 show the comparisons of computational and experimental results of temperature histories on the surface of the sensor for the one-layer shell fabric with and without an air gap, respectively. Six-second exposure was applied to the test configuration with an air gap and 3-s exposure to the one without an air gap. Overall agreement can be observed from these comparisons of model prediction and experimental results. However, in Figure 4 (the configuration without an air gap) the temperature rise predicted by the model is relatively lower

TABLE 1. Thermophysical/Geometrical Properties of the Fabric [2]

Property	Symbol	Unit	Outer Shell:	Moisture Barrier:	Thermal Liner:
			Kombat™ 7.5 oz/yd ²	ComfortZone™	Aralite®
Fiber density	ρ_{ds}	kg·m ⁻³	1384	1295	1380
Fiber specific heat	$(c_p)_{ds}$	J·kg ⁻¹ ·K ⁻¹	1420	1325	1200
Fiber thermal conductivity	k_{ds}	W·m ⁻¹ ·K ⁻¹	0.179	0.144	0.130
Thickness	L	m	0.56×10^{-3}	0.73×10^{-3}	1.66×10^{-3}
Fiber volume fraction	ϵ_{ds}		0.334	0.186	0.115
Fiber regain at 65% relative humidity	R_f		0.084	0.038	0.045
Tortuosity	τ		1.50	1.25	1.00
Ratio of effective diffusivity of bound water in the fiber to average fiber diameter	D_{solid} / d_f^2	s ⁻¹	2.34×10^{-4}	2.34×10^{-4}	2.34×10^{-4}
Interfacial conductance between inner surface of fabric and sensor	h_i	W·m ⁻² ·K ⁻¹	55.0	70.0	40.0

Notes. 7.5 oz/yd² = 254.3 g/m².

TABLE 2. Radiation Parameters [3]

Property	Symbol	Fabric	Flame	TPP Sensor
Emissivity	$\tilde{\epsilon}$	0.9	0.02	0.95
Transmissivity	$\tilde{\tau}$	0.01	—	—

Notes. TPP—thermal protective performance.

TABLE 3. Thermophysical/Geometrical Properties of the Thermal Protective Performance (TPP) sensor

Property	Symbol	Unit	TPP Sensor
Mass of copper	m	g	17.8
Specific heat of copper	c_p	cal/g·°C	0.0927
Surface area of copper	A	cm ²	12.56

TABLE 4. Initial Conditions for the Fabric and the Air Gap of the Thermal Protective Performance (TPP) Configuration Test, and the Thermal Properties of the Flame and the Ambient Air

Condition/Property	Symbol (Unit)	Unit	Value
Initial fabric temperature	$T_{0,fap}$	°C	26.0
Initial relative humidity in fabric	$\Phi_{0,fab}$	—	0.68
Initial relative humidity in air gap	$\Phi_{0,gap}$	—	0.68
Initial sensor temperature	$T_{0,sens}$	°C	28.0
Ambient temperature	T_{amb}	°C	26.0
Ambient relative humidity	Φ_{amb}		0.68
Convective heat transfer coefficient between flame and outer surface of fabric	$h_{c,fl}$	W·m ⁻² ·K ⁻¹	120
Flame temperature	T_{fl}	°C	1450
Convective mass transfer coefficient in air gap	$h_{m,gap}$	m·s ⁻¹	0.021
Ambient convective mass transfer coefficient	$h_{m,amb}$	m·s ⁻¹	0.021
Total gas phase pressure	p_γ	N·m ⁻²	1.01325×10^5
Thickness of air gap	L_{gap}	m	6.35×10^{-3}

than the experimental data before 10 s and higher after 10 s. This may be because vaporized moisture as a result of temperature gradient moves towards the sensor and condensates on the surface of the sensor. In the experiment, there

was condensation water on the surface of the sensor. Figures 5 and 6 compare computational and experimental results for the two-layer fabric system. The exposure times applied in Figure 5 (with an air gap) and Figure 6 (without

an air gap) are 7.2 and 14.2 s, respectively. The computation curve predicts a higher temperature rise comparing with experimental data in both configurations, particularly after 10–20 s from the start of exposure. The moisture barrier in this fabric system may contribute to the difference between computational and experimental results. In the model, the nature of moisture transfer in the barrier layer was not considered and the assumption was the same as that used in the case of textile layers. In Figures 7 and 8, computational and experimental results for the multilayer fabric are compared for different test configurations. The exposure times for the multilayer fabric were

23 s for the configuration with an air gap and 15 s for the one without an air gap. The comparisons in Figures 7 and 8 demonstrate good agreement between model predictions and experimental tests under both test configurations. The effect of the moisture barrier layer, like in the two-layer system, was minimized in the multilayer system as a result of the addition of a thicker thermal insulation layer. The exposure times for these fabric systems were selected on the basis of the estimation of energy transferred through a fabric system and air layers that could cause second-degree burn.

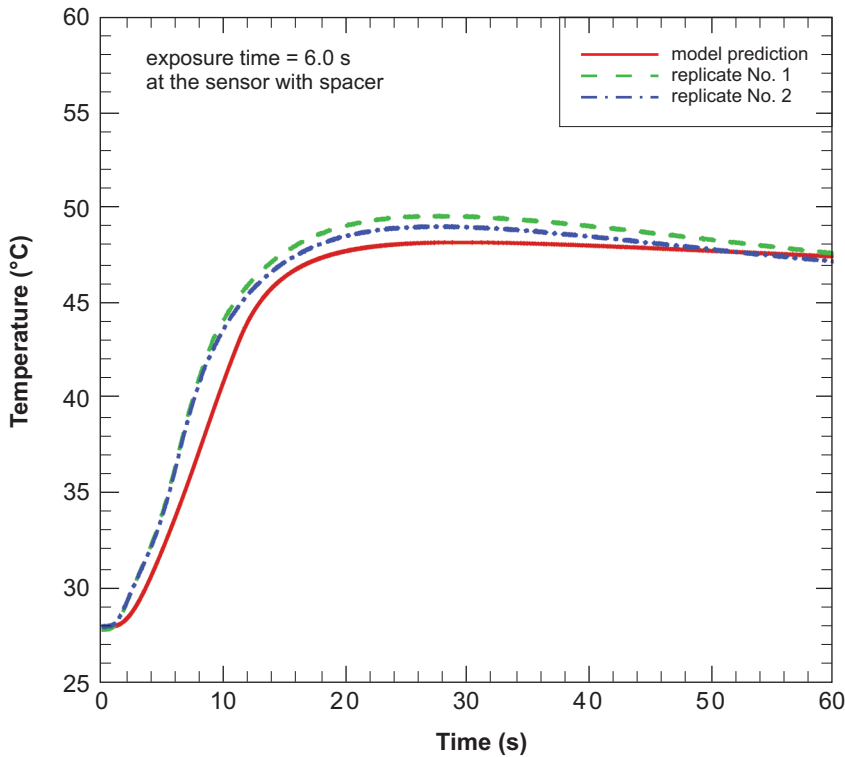


Figure 3. Comparison of computational and experimental results of temperature histories on the surface of the sensor for a one-layer system (Kombat™ 7.5 oz/yd²) with an air gap.

Notes. 7.5 oz/yd² = 254.3 g/m².

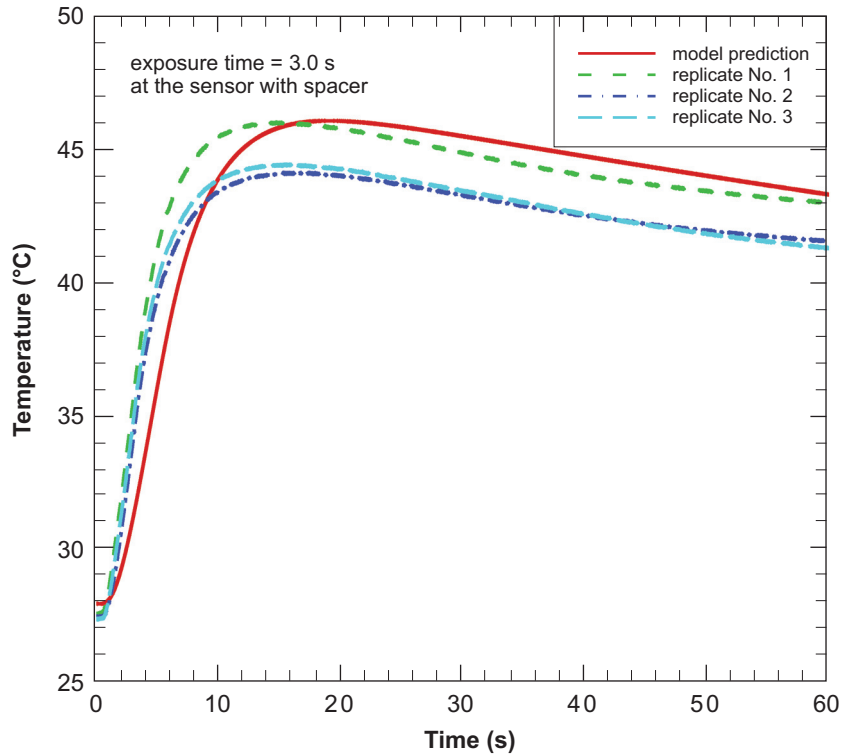


Figure 4. Comparison of computational and experimental results of temperature histories on the surface of the sensor for a one-layer system (Kombat™ 7.5 oz/yd²) without an air gap. Notes. 7.5 oz/yd² = 254.3 g/m².

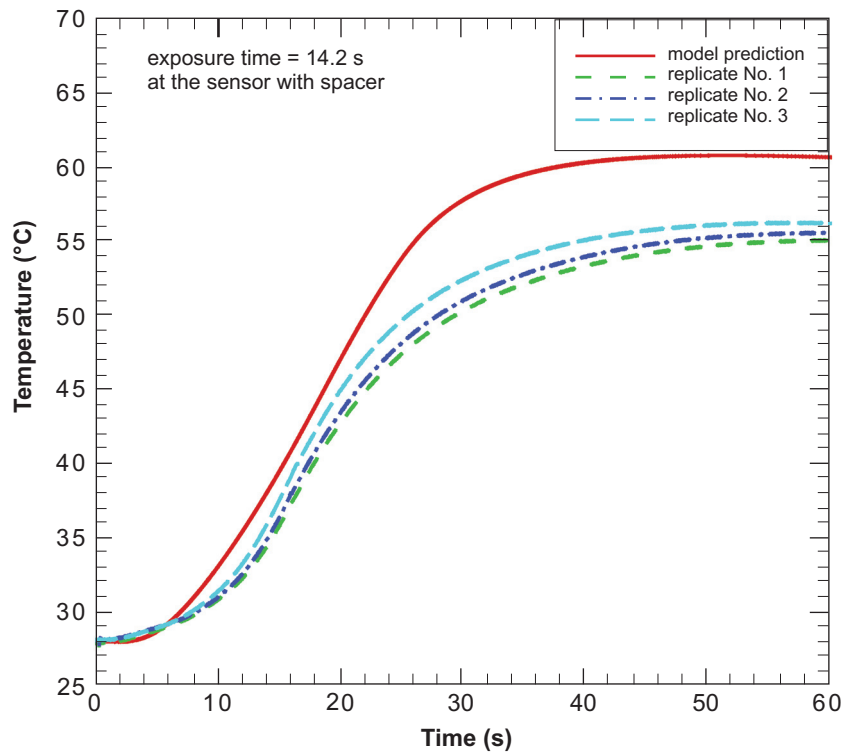


Figure 5. Comparison of computational and experimental results of temperature histories on the surface of the sensor for a two-layer (Kombat™ 7.5 oz/yd², ComfortZone™) system with an air gap. Notes. 7.5 oz/yd² = 254.3 g/m².

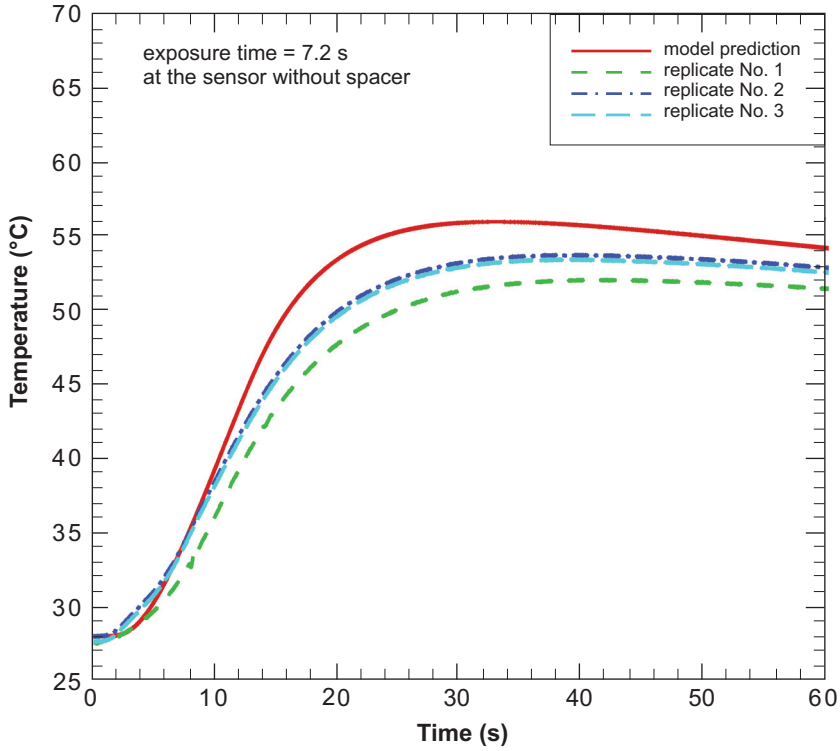


Figure 6. Comparison of computational and experimental results of temperature histories on the surface of the sensor for a two-layer system (Kombat™ 7.5 oz/yd², ComfortZone™) without an air gap. Notes. 7.5 oz/yd² = 254.3 g/m².

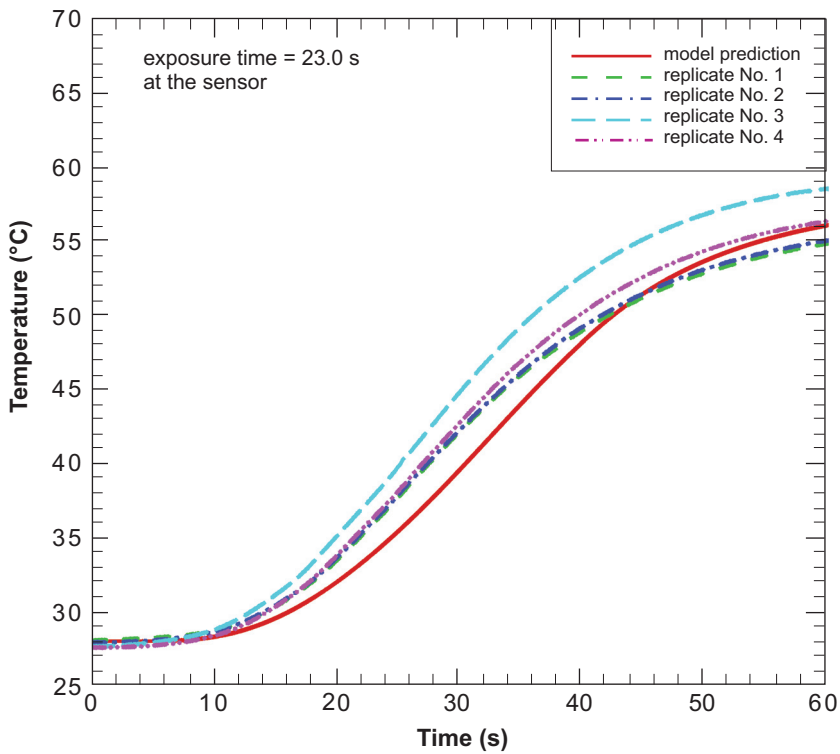


Figure 7. Comparison of computational and experimental results of temperature histories on the surface of the sensor for a two-layer (Kombat™ 7.5 oz/yd², ComfortZone™, Aralite®) system with an air gap. Notes. 7.5 oz/yd² = 254.3 g/m².

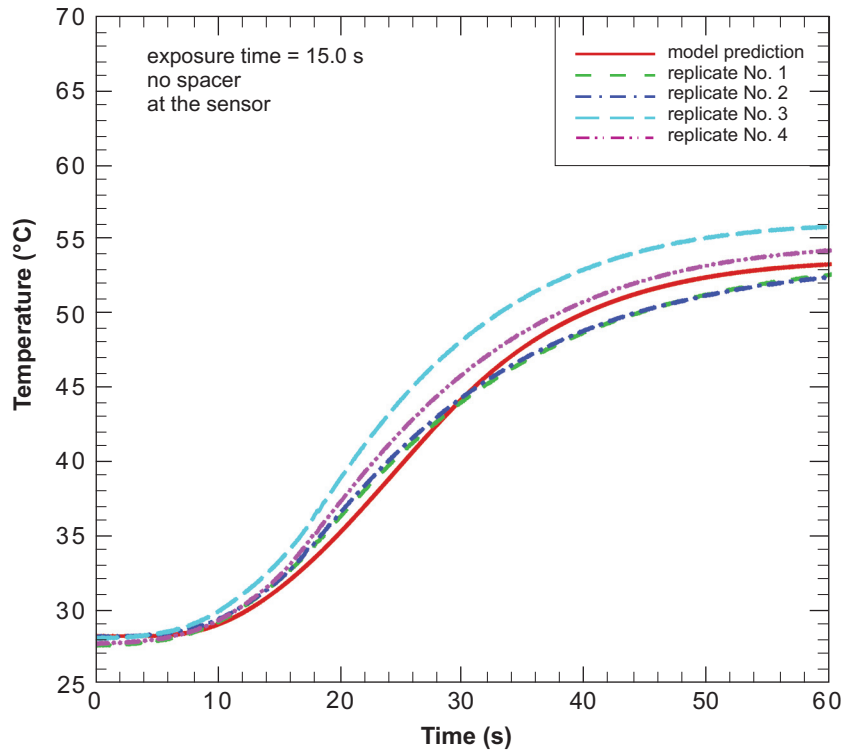


Figure 8. Comparison of computational and experimental results of temperature histories on the surface of the sensor for a three-layer (Kombat™ 7.5 oz/yd², ComfortZone™, Aralite®) system without an air gap. Notes. 7.5 oz/yd² = 254.3 g/m².

4. MODEL APPLICATION

4.1. Temperature and Moisture Distribution

Predictions from the established model are performed for the duration of 4-s exposure to a flash fire, with an introduction of an air gap. The air gap is 0.00635 m (1/4 in.) long. To examine the heat and moisture transfer feature during the cooling period (postexposure), computations continue until 60 s after the end of exposure. The temperature of the hot gas and the ambient temperature gradually decrease after 4 s of burning [17]. From the expression for the Nusselt number, natural convection will contribute to heat transfer across the enclosure when the Rayleigh number, Ra , is greater than 1708. The maximum Rayleigh number, for all computed cases of the TPP test was 1123. Therefore, for the case computed in this paper, Ra is always smaller than 1708, which means that natural

convection is negligible. Therefore, radiation and conduction heat transfer will dominate heat transfer mechanisms across the air gap.

Figure 9 describes temperature distribution predicted by the numerical model in a multilayer fabric, the air gap, and the sensor at different moments of time. Distance in Figure 9 represents the thickness of the fabric composite (0–2.95 mm) and the size of the air gap (2.95–9.20 mm). The end of the distance, at 9.20 mm, represents the surface of the sensor. During 4-s exposure, the surface temperature of the fabric of the outer shell rises fast, from room temperature to more than 400 °C, and maximum temperature can be observed at the outer surface of the fabric at ~4 s. After exposure, surface temperature falls slowly and in ~60 s surface temperature drops back to a point that is very close to room temperature. In comparison to the temperature on the outer surface of the fabric, the temperature on the inner surface of the fabric increases slowly and maximum temperature is predicted at ~10 s in 4-s exposure to flash fire.

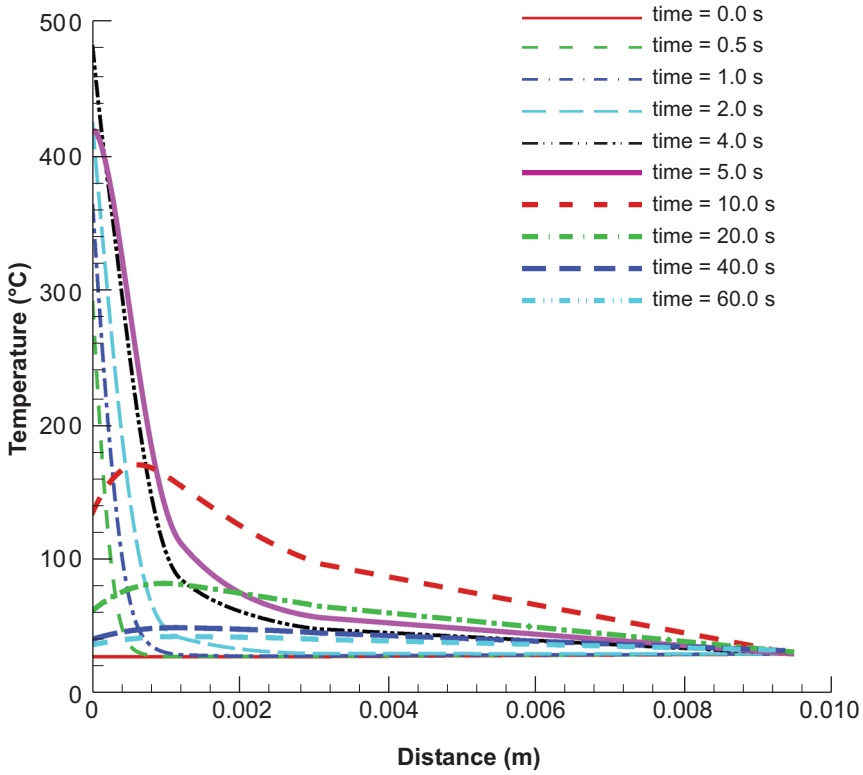


Figure 9. Temperature distribution in the fabric, the air gap, and the sensor at different times.

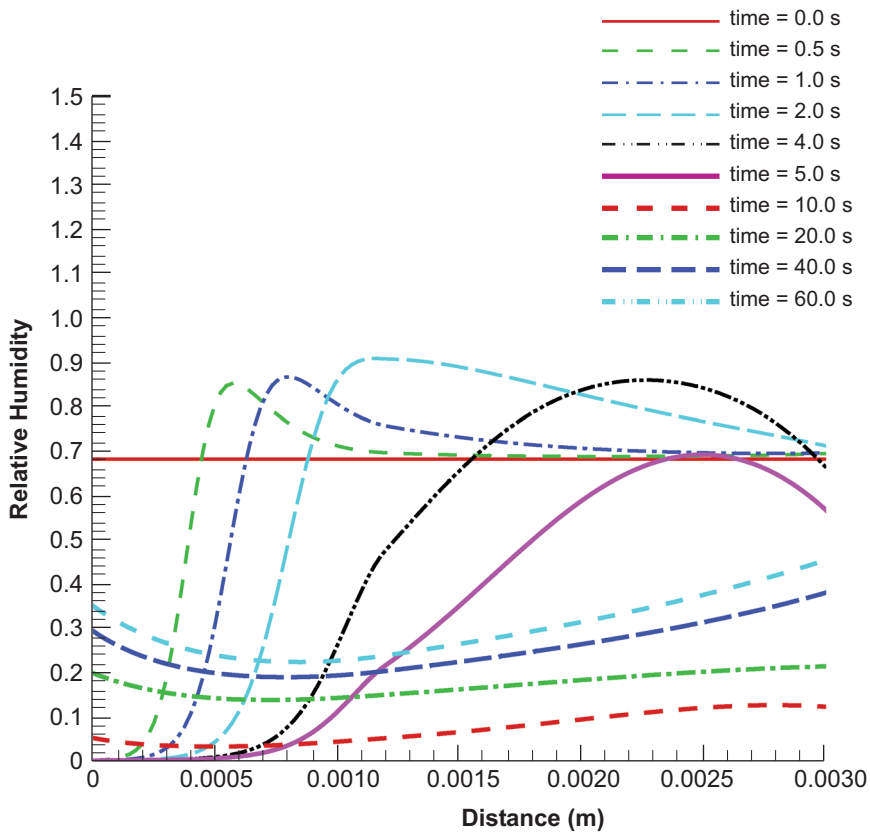


Figure 10. Distribution of relative humidity in the fabric at different moments of time.

This phenomenon indicates that energy stored during exposure moves towards the back of the fabric layers during the postexposure period. A significant temperature difference is predicted between the inner layer of the fabric and the surface of the sensor.

Figure 10 depicts distribution of relative humidity in the fabric (vapor in gas phase in the fabric as shown in Figure 2) at different moments of time. Relative humidity in the outer layer of garment decreases significantly when exposure to flash fire starts and it increases in the latter layers. This indicates that the moisture vaporized in the outer layer moves towards the inside fabric layer and eventually into the air gap because of the temperature gradient as described in Figure 9. At ~10 s, the model predicts minimum relative humidity in the fabric system; then the fabric system gradually regains its moisture. After the temperatures on the outer surface and the inner surface of the fabric become low enough, relative humidity starts growing back to its initial distribution.

In Figure 11 the distribution of fiber moisture regain in the fabric (bound water in the solid phase as shown in Figure 2) at different moments of time are investigated. Regain is defined as the ratio of the mass of absorbed water in the fiber to the mass of dry fiber. At the beginning the fiber in the fabric is in the state of equilibrium. Fiber regain in the fabric decreases during 4-s exposure to the flash fire and it continues to decrease until minimum values are achieved, which corresponds to equilibrium at those temperature and relative humidity conditions. If the cooling time is long enough, both fiber regain and moisture content in the fabric will go back to what they were at the initial state.

Figure 12 presents distribution of vapor density in the multilayer fabric at different moments of time. Vapor density increases because temperature increases and causes the phase transition from bound water to water vapor. In addition, as the temperature gradient develops during exposure, moisture in the outer layer moves towards the inner layer and contributes to the change in vapor density.

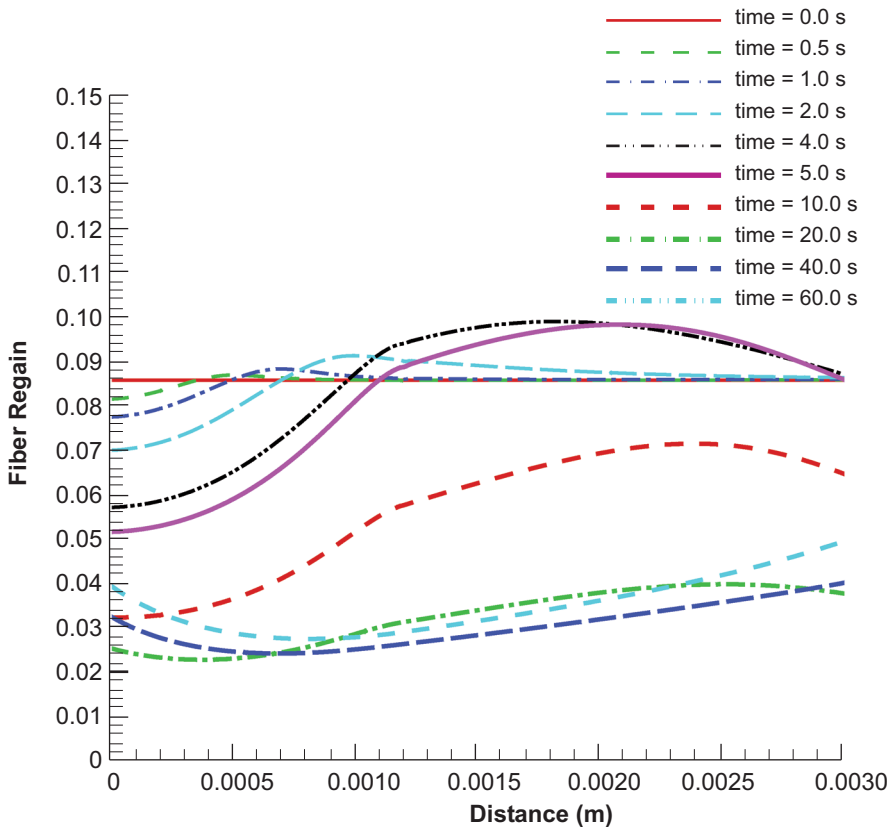


Figure 11. Distribution of fiber moisture regain in the fabric at different moments of time.

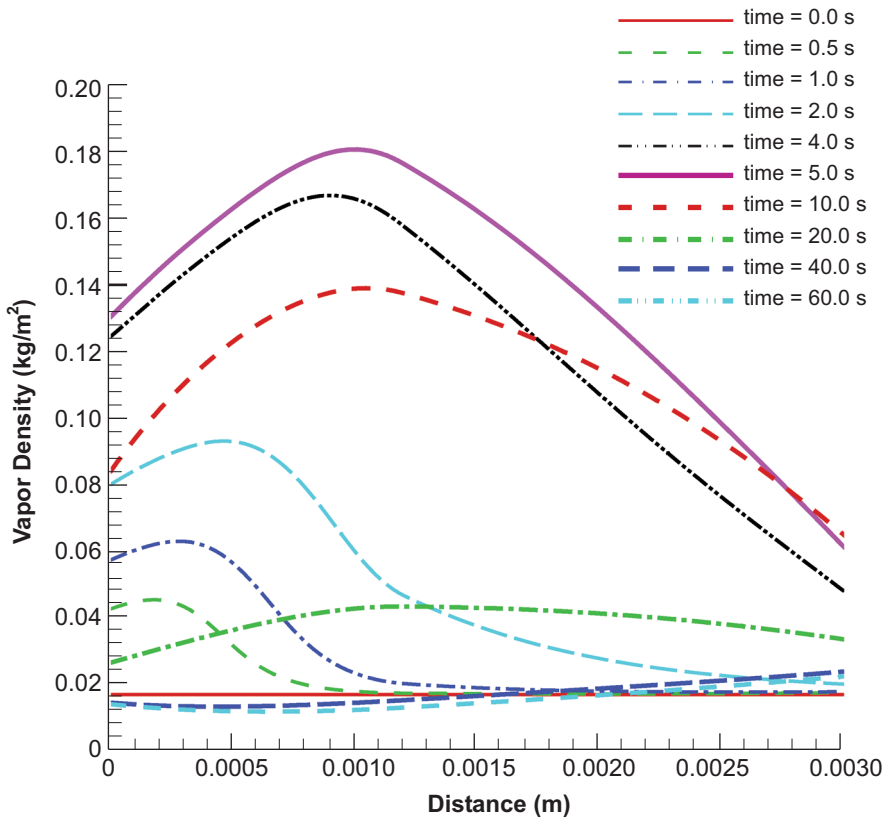


Figure 12. Distribution of vapor density in the fabric at different moments of time.

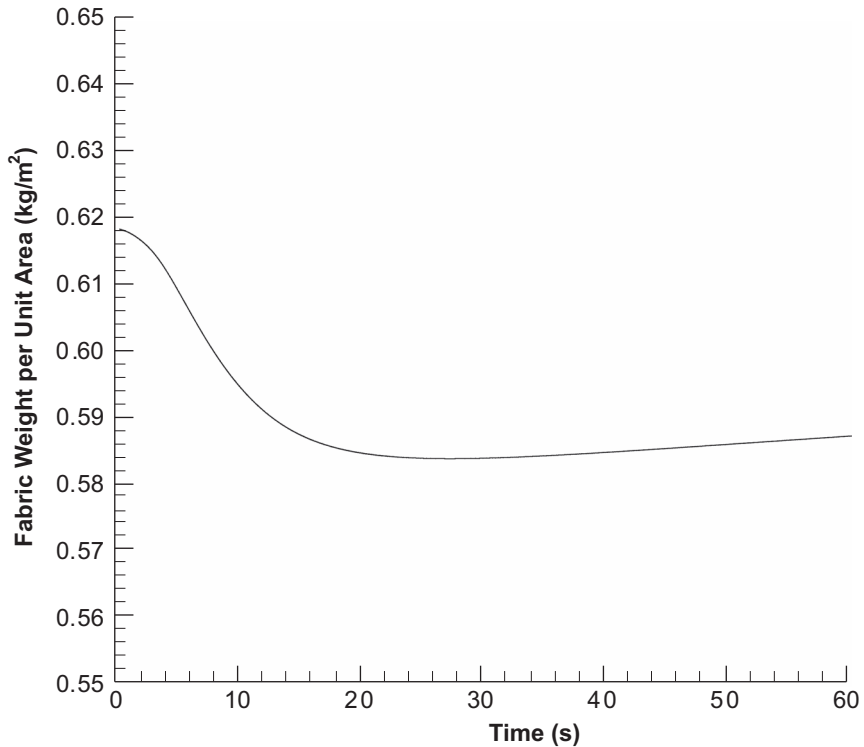


Figure 13. Predicted change in fabric weight during and after exposure.

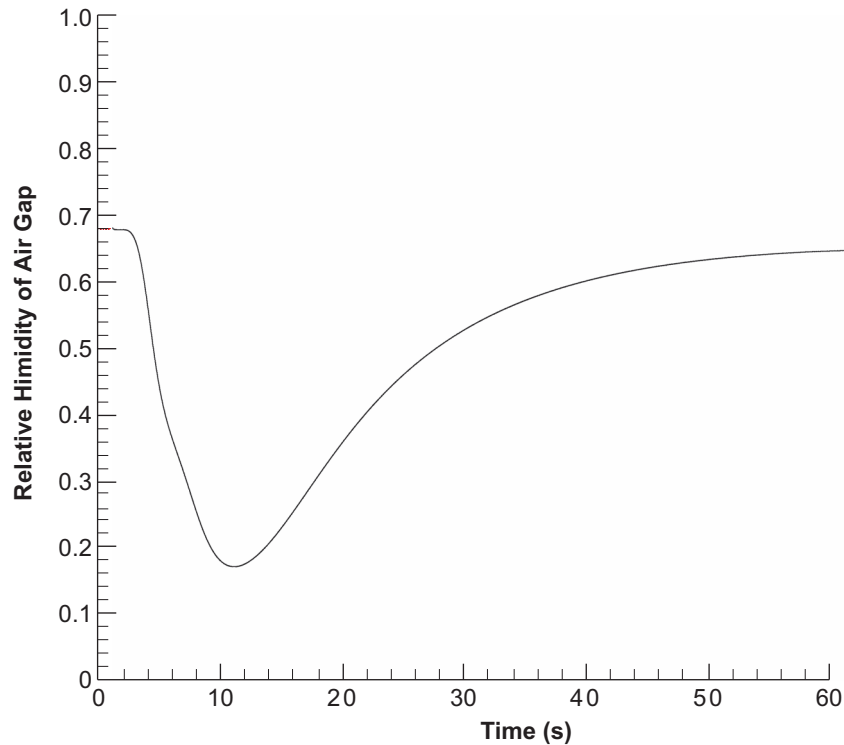


Figure 14. Predicted change in relative humidity in the air gap during and after exposure.

The calculated fabric weight per unit area during and after exposure is examined in Figure 13. It shows that fabric weight decreases significantly during the first 20 s. This is mainly because when temperature increases, moisture (bound water) in the fiber vaporizes and moves into the air gap. This phenomenon relates well to the change in fiber moisture regain as shown in Figure 11, which shows that minimum fiber moisture regain can be obtained after 20 s.

Figure 14 presents the predicted change in relative humidity in the air gap during and after exposure. After 4-s exposure relative humidity drops significantly and reaches the minimum at ~10 s from the start of exposure. From Figure 9 the model predicts temperature change in the air gap and higher temperature can be observed at ~10 s. When temperature increases, saturation pressure also increases. Therefore, relative humidity in the air gap decreases even though the moisture content in the air gap increases.

4.2. Effects of Variations on Clothing Protective Performance

The three-layer skin model was used to predict the performance of a thermal protective fabric system in terms of skin burn. It was based on Henriques and Moritz's work, which shows that destruction of the tissue layer located at the epidermis/dermis interface in human skin starts when the tissue temperature of the basal layer rises above 44 °C [18]. The destruction rate can be modeled using a first-order chemical reaction, i.e.,

$$\frac{d\Omega}{dt} = P \exp\left(-\frac{\Delta E}{RT}\right), \quad (15)$$

where Ω —quantitative measure of burn damage at the basal layer or at any depth in the dermis; P —frequency factor, s^{-1} ; E —activation energy for skin, J/mol; R —universal gas constant, 8.315 J/kmol·K; T —absolute temperature at the basal layer or at any depth in the dermis, K; t —total time for which T is above 44 °C (317.15 K).

Integration of this equation yields

$$\Omega = \int_0^t P \exp\left(-\frac{\Delta E}{RT}\right) dt. \quad (16)$$

Integration is performed from the time when the temperature of the basal layer of the skin, T , exceeds or equals 44 °C. Henriques found that if $\Omega \leq 0.5$, no damage will occur at the basal layer [18]. If Ω is 0.5–1.0, there will be first-degree burns, whereas if $\Omega > 1.0$, second-degree burns will result. The damage criteria can be applied to any depth of skin provided appropriate values of P and ΔE are used. Mathematically, a second-degree burn has been defined as $\Omega > 1.0$ at the epidermis/dermis interface. Details about the structure of the skin model as well as the properties and parameters used for Henriques’ burn integral are given in the Appendix on p. 106.

Table 5 illustrates the prediction of protective performance for the three-layer clothing system with different sizes of the air gap. Table 1 lists the properties used in the numerical model. Minimum exposure time required to develop a second-degree burn was predicted. The results show that with the typical air gap size of 0.00635 m (1/4 in.), minimum exposure time was predicted at 10.3 s under exposure to flash fire. For the selected air gap range of 1.59–6.35 mm, the model predicts a significant decrease in minimum exposure time when the size of the air gap decreases. As air is a good insulator, decreasing the size of the air gap will decrease the value of insulation provided by the air layer between the fabric and the skin. However, when the air gap was increased beyond 6.35 mm, no significant change in minimum exposure time was observed. This agrees with Song’s [19] study that during exposure to a flash fire (84 kW/m²) natural convection may occur in the air gap between the clothing and human skin (sensor). When the air gap is large, convection increases the amount of energy transferred to the skin.

TABLE 5. Air Gap Size and Minimum Exposure Time Required to Generate a Second-Degree Burn

Air Gap Size (m)	Minimum Exposure Time (s)
0.00159	7.7
0.00318	9.1
0.00635	10.3
0.01270	10.7

The effect of fiber density, conductivity, and capacity on the protective performance of clothing was investigated. As different fibers were used in shell fabrics and thermal liners, different ranges of values of properties were selected. Table 6 demonstrates the effect of a change in fiber density on the protective performance of clothing. The predictions were made by changing the fiber density in the numerical model while other parameters were the same as those employed in the model. The results showed that increasing fiber density of shell fabrics and thermal liners, improved thermal protective performance. In the model the effective density of the fabric was employed, which is a combination of the density of the fiber, moisture, and trapped air in the fabric. Therefore, a change in fiber density affects the effective density of the fabric. An increase in fabric effective density causes lower fabric thermal diffusivity, hence heat transfer in the fabric system slows down and consequently improved protective performance is predicted. A change in fiber conductivity and thermal capacity affects thermal protective performance as illustrated in Tables 7 and 8. This was achieved by changing one parameter and leaving the others the same as in the numerical model. As described in the development of the model, the fabric was modeled as porous media and the system consisted of fiber, trapped air, and moisture. A large part of the insulation of the thermal liner was provided by the air trapped in the fabric. Therefore, change in fiber conductivity and specific heat capacity within a certain range did not significantly affect heat transfer as expected. The results obtained from the numerical model, as shown in Tables 7 and 8, confirm this. However, the overall trend shows that increasing fiber conductivity affects heat flow in the system and causes skin temperature to rise faster. As a result, minimum exposure time decreases as fiber thermal conductivity increases. For fiber specific heat capacity, the model results indicate that minimum exposure time increases with an increase in fiber specific heat capacity. It should be noted that the model analysis does not include fiber decomposition reactions and its effect on heat and mass transfer.

TABLE 6. Fiber Density and Predicted Minimum Exposure Time Required to Generate a Second-Degree Burn

Fiber Density ($\text{kg}\cdot\text{m}^{-3}$)		Minimum Exposure Time (s)
Shell Fabric	Thermal Liner	
1107	1104	9.7
1384	1380	10.3
1661	1656	11.0
2076	2070	12.1

TABLE 7. Fiber Thermal Conductivity and Predicted Minimum Exposure Time Required to Generate a Second-Degree Burn

Fiber Thermal Conductivity ($\text{W}\cdot\text{m}^{-1}\cdot\text{K}^{-1}$)		Minimum Exposure Time (s)
Shell Fabric	Thermal Liner	
0.143	0.104	10.8
0.179	0.130	10.3
0.215	0.156	10.0
0.269	0.195	9.6

TABLE 8. Fiber Specific Heat Capacity and Predicted Minimum Exposure Time Required to Generate a Second-Degree Burn

Fiber Specific Heat Capacity ($\text{J}\cdot\text{kg}^{-1}\cdot\text{K}^{-1}$)		Minimum Exposure Time (s)
Shell Fabric	Thermal Liner	
1136	960	9.8
1420	1200	10.3
1704	1440	10.9
2130	1800	11.8

The results obtained from the numerical model suggest that the thickness of the fabric significantly affects its thermal protective performance. Table 9 reports on the thermal protective performance of fabric systems with different thickness of shell and thermal liners: an increase in fabric thickness significantly increases

TABLE 9. Fabric Thickness and Predicted Minimum Exposure Time Required to Generate a Second-Degree Burn

Thickness (mm)		Minimum Exposure Time (s)
Shell Fabric	Thermal Liner	
0.45	1.33	7.8
0.56	1.66	10.3
0.67	1.99	13.3
0.84	2.46	21.0

minimum exposure time. An increase in fabric thickness provides better insulation and when there is exposure, the temperature difference between the exposed and skin sides of the fabric increases. Additionally, during exposure, a thicker fabric normally stores more thermal energy than a thinner one; therefore, energy transfer to human skin (or a sensor) is lower.

The effects of the initial temperature of a fabric and of environmental conditions on the performance of protective clothing were examined using the numerical model. Table 10 lists the results of model predictions with different initial temperatures of a fabric; a clothing system can provide more protection if the initial temperature of the fabric is relatively low. Comparatively, when exposed to a thermal hazard, the fabric at a lower temperature will store more energy than a fabric system at a higher temperature and it will generate a slow temperature rise on the side of the skin. As a result, the fabric system will perform better. Moisture regain in the fiber changes both fiber conductivity and specific heat, and during intense thermal conditions a hot stream, which contributes to human skin burn, is generated. Table 11 shows that the effect of moisture on minimum exposure time is minor when fiber moisture regain is relatively low. When it is high, however, minimum exposure time is higher.

TABLE 10. Initial Temperature of the Fabric and Predicted Minimum Exposure Time Required to Generate a Second-Degree Burn

Initial Temperature ($^{\circ}\text{C}$)	Minimum Exposure Time (s)
5	11.4
26	10.3
35	9.7
50	8.5

TABLE 11. Fabric Moisture Regain and Predicted Minimum Exposure Time Required to Generate a Second-Degree Burn

Fiber Moisture Regain (%)		Minimum Exposure Time (s)
Shell Fabric	Thermal Liner	
16.8	9.0	10.9
8.4	4.5	10.3
4.8	2.3	10.2
2.4	1.1	10.1

5. CONCLUSIONS

A numerical model of coupled heat and moisture transport in protective clothing during exposure to a flash fire was investigated and compared with experimental results. This model can be used to predict the thermal response of a protective fabric when it is exposed to a flash fire. It can also be used to obtain the distribution of temperature and moisture as well as information on the effect of some properties of fabrics and an air gap on protective performance under exposure to a flash fire. A typical three-layer protective clothing system provides protection during ~9–12-s exposure to a flash fire, without causing a second-degree burn. An air gap layer between the fabric and the skin provides extra insulation and slows down heat transfer to the skin. The thickness of the fabric system is an important factor in the performance of thermal protective clothing.

REFERENCES

1. Bouddour A, Auriault JL, Mhamdi-Alaoui M. Heat and mass transfer in wet porous media in presence of evaporation–condensation. *Int J Heat Mass Transfer*. 1998;41(15):2263–77.
2. Stull JO. The effect of moisture on firefighter protective clothing thermal insulation: review of industry research. In: Nelson CN, Henry NW, editors. *Performance of protective clothing (ASTM STP 1386)*. West Conshohocken, PA, USA: American Society for Testing and Materials (ASTM); 2000. p. 557–76.
3. Lee YM, Barker RL. Effect of moisture on the thermal protective performance of heat-resistant fabrics. *J Fire Sci*. 1986;4(5): 315–31.
4. Barker RL, Guerth-Schacher C, Grimes RV, Hamouda H. Effects of moisture on the thermal protective performance of firefighter protective clothing in low-level radiant heat exposures. *Text Res J*. 1996;76(1):27–31.
5. Lawson JR. Fire fighters' protective clothing and thermal environments of structural fire fighting. In: Stull JO, Schwobe AD, editors. *Performance of protective clothing (ASTM STP 1273)*. West Conshohocken, PA, USA: American Society for Testing and Materials (ASTM); 1997. p. 334–52.
6. Crow RM, Osczevski RJ. The interaction of water with fabrics. *Text Res J*. 1998;68(4): 280–8.
7. Vafai K, Sözen M. A comparative analysis of multiphase transport models in porous media. In: Tien CL, editor. *Annual Review of Heat Transfer*. Vol. 3. New York, NY, USA: Hemisphere; 1990. p. 145–62.
8. Gibson PW. Multiphase heat and mass transfer through hygroscopic porous media with applications to clothing materials (Technical report Natick/TR-97/005). Natick, MA, USA: U.S. Army Natick Research, Development, and Engineering Center; 1996.
9. Torvi DA. Heat transfer in thin fibrous materials under high heat flux conditions [doctoral dissertation]. Edmonton, Canada: University of Alberta; 1997.
10. Whitaker S. Simultaneous heat, mass, and momentum transfer in porous media: a theory of drying. In: Hartnett JP, Irvine Jr TF, editors. *Advances in Heat Transfer*. Vol. 13. New York, NY, USA: Academic Press; 1977. p. 119–203.
11. Morton W, Hearle J. *Physical properties of textile fibres*. Manchester, UK: The Textile Institute; 1993.
12. Hollands KGT, Unny TE, Raithby GD, Konicek L. Free convective heat transfer across inclined air layers. *J Heat Transfer*. 1976;98:189–93.
13. Chitrphiomsri P, Kuznetsov AV. Modeling heat and moisture transport in firefighter protective clothing during flash fire exposure. *Heat Mass Transfer*. 2005;41:206–15.
14. Patankar SV. *Numerical heat transfer and fluid flow*. Washington, DC, USA: Taylor & Francis; 1980.
15. Tannehill JC, Anderson DA, Pletcher RH. *Computational fluid mechanics and heat transfer*. Washington, DC, USA: Taylor & Francis; 1997.
16. American Society for Testing and Materials (ASTM) Standard test method for thermal protective performance of materials for clothing by open-flame method (ASTM D

- 4108-87). West Conshohocken, PA, USA: ASTM; 1987.
17. Song G, Barker R, Hamouda H, Kuznetsov A, Chittrphiromsri P, Grimes R. Modeling the thermal protective performance of heat resistant garments in flash fire exposures. *Text Res J.* 2004; 74(12):1033–40.
 18. Henriques FC Jr, Moritz AR. Studies of thermal injuries I: the conduction of heat to and through skin and the temperatures attained therein. A theoretical and experimental investigation. *Am J Pathol.* 1947;23:531–49.
 19. Song G. Clothing air gap layers and thermal protective performance in single layer garment. *J Ind Text.* 2007;36(3):139–205.
 20. Stoll AM, Greene LC. Relationship between pain and tissue damage due to thermal radiation. *J Appl Physiol.* 1959;14(3):373–82.
 21. Takata A. Development of criterion for skin burns. *Aerosp Med.* 1974;45(6):634–7.

APPENDIX

A three-layer skin model was used in this study. Table 12 summarizes the thermophysical properties of the skin layer.

TABLE 12. Skin Properties in a Three-Layer Skin Model

Human Skin	Property	Value
Epidermis	thermal conductivity (W/m.°C)	0.255
	density (kg/m ³)	1200
	specific heat (J/kg.°C)	3598
	thickness (m)	8.0 × 10 ⁻⁵
Dermis	thermal conductivity (W/m.°C)	0.523
	density (kg/m ³)	1200
	specific heat (J/kg.°C)	3222
	thickness (m)	2.0 × 10 ⁻³
Subcutis	thermal conductivity (W/m.°C)	0.167
	density (kg/m ³)	1000
	specific heat (J/kg.°C)	2760
	thickness (m)	1.0 × 10 ⁻²

The values of *P* and ΔE in Equation 16 are from Stoll and Greene [20] and Takata [21]:

epidermis
 for $T < 50\text{ }^{\circ}\text{C}$ $P = 2.185 \times 10^{124} \text{ s}^{-1}$, $\Delta E/R = 93\,534.9 \text{ K}$;
 for $T \geq 50\text{ }^{\circ}\text{C}$ $P = 1.823 \times 10^{51} \text{ s}^{-1}$, $\Delta E/R = 39\,109.8 \text{ K}$;

dermis
 for $T < 50\text{ }^{\circ}\text{C}$ $P = 4.32 \times 10^{64} \text{ s}^{-1}$, $\Delta E/R = 50\,000 \text{ K}$;
 for $T \geq 50\text{ }^{\circ}\text{C}$ $P = 9.39 \times 10^{104} \text{ s}^{-1}$, $\Delta E/R = 80\,000 \text{ K}$.